Inlaid microfluidic optics: absorbance cells in clear devices applied to nitrite and phosphate detection

OPEN ACCESS
IOP Publishing
Journal of Micromechanics and Microengineering
J. Micromech. Microeng. **30** (2020) 095001 (15pp)
https://doi.org/10.1088/1361-6439/ab9202

Inlaid microfluidic optics: absorbance cells in clear devices applied to nitrite and phosphate detection

Edward A Luy, Sean C Morgan, Joshua J Creelman, Benjamin J Murphy and Vincent J Sieben

Department of Electrical and Computer Engineering, Dalhousie University, 1360 Barrington Street, Halifax, Nova Scotia B3H 4R2, Canada

E-mail: Eddy.Luy@dal.ca and sieben@dal.ca

Received 30 March 2020
Accepted for publication 11 May 2020
Published 18 June 2020

Abstract

A novel type of microfluidic absorbance cell is presented here that inlays black poly(methyl methacrylate) (PMMA) into a clear PMMA substrate to realize an isolated optical channel with microlitre volumes. Optical measurements are frequently performed on microfluidic devices, offering effective, quick, and robust chemical analysis capabilities on small amounts of sample. Many lab-on-chip systems utilize micrometer-sized channels to analyze liquid samples via light-absorbance measurements, but this requires sophisticated coordination of light through a small cross-section, often requiring collimating and beam-steering optics. Here, we detail the fabrication process to realize long path length absorbance cells based on a simple hybrid-material approach. A z-shape microchannel structure crosses a clear-black interface at both ends of the absorbance cell, thereby creating integral optical windows that permit light coupling into a microchannel completely embedded in black PMMA. Furthermore, we have integrated v-groove prisms on either side of the microfluidic channel. The prisms enabled seamless integration with printed circuit boards and permit the optical elements to be located off-chip without use of epoxies or adhesives. Three path lengths, 10.4, 25.4, and 50.4 mm, were created and used to characterize the novel cell design using typical colorimetric measurements for nitrite and phosphate. We compare the attenuation coefficient measured by our optical cells with the literature, showing excellent agreement across nutrient concentrations from 50 nM–50 μM. The measurements were performed with well-known reagent-based methods, namely the Griess assay for nitrite and the molybdovanadophosphoric acid or the 'yellow method' for phosphate. The longest 50.4 mm path length cell had a limit-of-detection of 6 nM for nitrite and 40 nM for phosphate, using less than 12 μl of fluid. The inlaid fabrication method described permits robust and high-performance optical measurements with broad applicability for *in situ* marine sensors and for numerous lab-on-chip sensors based on colorimetric assays. One such application is shown whereby two inlaid absorbance cells are integrated with four microfluidic check valves to realize a complete lab-on-chip nitrite sensor.

Supplementary material for this article is available online

Keywords: absorbance cells, microfluidic, chip, nitrate/nitrite, phosphate, fabrication, PMMA

(Some figures may appear in colour only in the online journal)

1. Introduction

Microfluidic technologies have been successful in performing chemical analysis methods on automated and portable sensor systems. Several analytical techniques have been implemented on microfluidic devices, including fluorescence microscopy [1], electrophoresis [2], chemiluminescence [3], and Raman spectroscopy [4] among others [5]. Microfluidic implementation of these mainstay techniques has improved resource-efficiency by reducing sample and reagent volume usage per measurement. Fluid optimization is even more important for automated instruments or *in situ* sensors that are intended for remote deployments, which may span multiple years and/or perform thousands of measurements [6]. For example, comprehensive temporal and spatial monitoring of large, dynamic environments like the world's oceans is challenging. This is due to manual collection, preservation, storage and/or transportation of samples for analysis in an on-ship laboratory cabin or an on-shore facility. The high reliance on qualified labour and the cost to manually retrieve samples has resulted in marine environments being severely under-sampled. Ideally, resource efficient sensors would measure the sample at source, thereby negating the need for the above manual process.

Currently, key nutrients including nitrate, nitrite, and phosphate in water samples from marine environments are measured using benchtop autoanalyzers. While these conventional systems are capable of high-performance, typically nanomolar and micromolar detection limits [7], they are difficult to deploy *in situ* and use excessive amounts of sample and reagent. Microfluidic technologies have been applied to measure these nutrients *in situ* with reduced volume and reagent consumption. Many microfluidic sensors described in the literature rely on spectrophotometric methods to probe small volumes of fluid in microchannels. These approaches are inexpensive and yet reliable, making them suitable for automated chemical analysis in challenging environments. In the last 10 years there have been numerous examples of spectrophotometric sensing on microfluidic platforms in ocean/marine environments, measuring: nitrite [8–10], nitrate [8, 11], phosphate [12–16], ammonia [17, 18] chromium [19], iron/cobalt [20]; pH [21], and silicate [22]. The core component in each sensor is the design of low volume and long path length optical cells. This requires controlled alignment of light through the sample for detection without background interference from non-directional and/or ambient light.

A microfluidic absorbance cell may utilize screwed-in or epoxy-fixed fibers to couple light to/from on-chip waveguides and flow cells for sample inspection [18, 23]. However, fiber-based lab-on-chip sensor designs tend to be less transferrable from the lab to the field, where slight mechanical shocks/vibrations can result in reduced optical coupling and sensor measurement error. Further, respecting the necessary bend radius of fiber-based systems presents a physical integration challenge for compact sensors and miniaturization. Alternatively, low-cost robust optical absorbance measurements may be realized by using the chip material itself. Sieben *et al* formed a completely integrated absorbance cell in chips fabricated from carbon-doped (tinted) semi-transparent PMMA [9]. Using this approach, light transmittance and measurement was achieved through thin windows which permitted an LED light source and a photodiode detector to be directly coupled to a 2.5–10 cm fluid flow cell. When light does not pass through the fluid microchannel, it is mostly attenuated elsewhere on the chip. This optical cell has been successfully applied to various microfluidic sensors [8, 14, 24] that have been deployed in marine environments to acquire thousands of measurements over multi-month durations. While the tinted approach to realizing microchannel absorbance cells provided a reliable core component for lab-on-chip marine sensors, it is based on a challenging alignment and fabrication process. Either UV-curable or time setting two-part epoxies completely immerse the LED and photodiode to hold them in perfect alignment to the microchannel. This requires a skilled and tedious workflow during the manufacturing process of these devices, where measurements must be taken to ensure optical alignment.

Here, we address these manufacturability challenges with a novel 'inlaid' optical cell that does not rely on epoxies to align or hold the source and detector. Our inlaid optical cell is comprised of sections of opaque and transparent material to achieve light transmission through a microfluidic channel that is almost entirely isolated from background light interference. A z-shape microchannel structure crosses a clear-black interface at both ends of the absorbance cell, thereby creating integral optical windows that permit light coupling into a microchannel completely embedded in black PMMA. As shown in figure 1, black material surrounds the fluid sensing channel to ensure that light is transmitted from one side to the other exclusively through the channel. Our design uses v-groove prisms, like Grumann *et al* [25], to couple light into and out of the channel from an external light source to a detector. Instead of the large channel cross-section described in Grumann *et al* (1 mm deep $\times$ 10 mm wide $\times$ 10 mm long, 100 μl cell volume), our black/inlaid PMMA enables small channel cross-sections, hence, a small volume absorbance cell (0.6 mm deep $\times$ 0.4 mm wide $\times$ 10.4 mm long, 2.5 μl cell volume). Our novel inlaid absorbance cell currently uses 40 times less volume and can be pushed further with process optimization. A light-emitting diode (LED) light source is held above the first prism which directs light into the channel using total-internal-reflection (TIR). A photodiode detector is held above the second prism, which directs light from the inlaid

microchannel to the detector. This permits long path lengths on the order of 1–10 cm, while maintaining low sample volumes; e.g. a 50.4 mm cell has a volume of 12.1 μl. We also describe a complete fabrication process to realize microfluidic chips based on our inlaid approach and demonstrate a chip with three inlaid absorbance cells of different path lengths.

The efficacy of our design in figures 1(a) and (c) was evaluated with ray-tracing software (Zemax, Washington, USA) as shown in figure 1(b) and is described in the supplementary material (avaliable online at stacks.iop.org/JMM/30/095001/mmedia). The graphs depict light sourced from an uncollimated LED that is directed towards the first prism (labeled 1—figure 1(a)) and light that is measured from the second prism (labeled 2—figure 1(a)), after passing through a 25 mm inlaid microfluidic cell. Observed by the detector is a focused beam with a narrower spatial distribution and <10% of the intensity of the incident light. Collimating optics or fibers are unnecessary to saturate a simple light detector (e.g. TSL257) through even a 25 mm long path as in figure 1(d). As an alternative, light could also be coupled directly through the channel from the side of the chip, as is done with the tinted-approach [8, 9]. The prisms, while not necessary, were implemented for the benefit of applying and detecting light from the topside of the chip. Interfacing the optical elements through the topside permits the light source and detector to be soldered components on a printed circuit board (PCB). The PCB can be held directly above the chip for rapid signal processing without any external wiring/connectors. This design is highly manufacturable, as repeatable and robust optical alignment can be achieved through standard manufacturing practices of component placement on PCBs. Furthermore, our inlaid approach allows us to change the LED and photodiode combination for different chemistries on the same chip design without detaching the optics/epoxy fixatives that would risk damaging the microfluidic chip. The supplementary material details simulations of light-absorbance measurements of a 25 mm long optical cell using prisms that confirm the benefits of inlaying opaque material around the optical cell to reduce detection of background non-directional light.

1.1. Application to nutrient detection

To validate our novel optical cell, we measured two nutrients fundamental to aquatic ecosystems: nitrite and phosphate. Light-absorbance measurements of nitrite samples reacted with the 'Griess' reagent is considered a gold-standard approach and has been described in great detail elsewhere [26, 27]. Under acidic conditions, a purple azo dye with peak absorbance near 540 nm will form in the presence of nitrite. Using a monochromatic light source centered near the peak of the azo dye absorbance spectra, nitrite has been measured to a limit-of-detection (LOD) in the nanomolar range [8, 9]. Phosphate detection is enabled using an acidic ammonium molybdate/metavanadate based reagent, hereby referred to as *phosphate reagent,* which forms a yellow complex proportional to phosphate concentration with maximum absorbance in the UV region [28] at 375 nm [29]. With both chemistries, we show that our inlaid microfluidic absorbance cell produced results in agreement with the literature for three different optical path lengths: 10.4, 25.4, and 50.4 mm. Following validation of the optical cell as an isolated system, a custom lab-on-chip nitrite sensor was successfully built to measure nitrite using both a 10 mm and a 25 mm inlaid optical cell integrated with 4 on-chip check valves.

2. Theory

In the work presented here, light-absorbance measurements are enabled by transmitting light from an LED through various fluids contained in a microfluidic channel to a light-to-voltage converter (photodiode) for detection. To couple light into and out of the channel, we employ prisms. According to Snell's law, light of wavelength λ will TIR at the PMMA–air prism interface, so long as the angle of incidence θ_i exceeds the critical angle θ_c:

$$\theta_c = \sin^{-1}\left(\frac{n_2(\lambda)}{n_1(\lambda)}\right) \tag{1}$$

where $n_1(\lambda)$ and $n_2(\lambda)$, the refractive indices of PMMA and air, are functions of the light wavelength λ. As such, we select the angle of the interface to be 45° to the incident beam on both prisms to satisfy the reflection condition while allowing both source and detector to be held perpendicular to the chip. This design choice allows for simple alignment between optical components and the chip, while also enabling a future design whereby optical components may be soldered to the bottom of a PCB mounted above the chip.

2.1. Absorbance spectroscopy

Absorbance spectroscopy is a common and well-established technique for biological and chemical analysis, either in continuous or stopped-flow configurations [30]. It is a simple, quick, and robust method of detecting the presence of a species within a fluid sample provided the analyte concentration is relatively low and that it has an accessible/unique absorbance spectrum. Incident light passing through a sample will attenuate depending on the molecular absorbance spectrum of the sample, the scattering from particles in the fluid, and the spectrum of incident light. For molecular absorbance, the molecules within the analyte may become excited and thus absorb energy from the incident waves as electrons are promoted to higher energy bands. The relative drop in light energy—or equivalently its intensity—can be used to calculate the absorbance of the sample using the Beer–Lambert law,

$$A = -\log_{10}\left(\frac{I}{I_0}\right) = \epsilon l c, \tag{2}$$

where absorbance A depends on the ratio of incident to transmitted light intensities, I_0 and I, respectively. The intensities are used to find the concentration c of the absorbing species as a function of the optical path length l and the attenuation coefficient of the analyte [31]. Here, we can largely ignore the effects of scattering attenuation as our fluid samples are sufficiently filtered. The Beer–Lambert law is intended for dilute

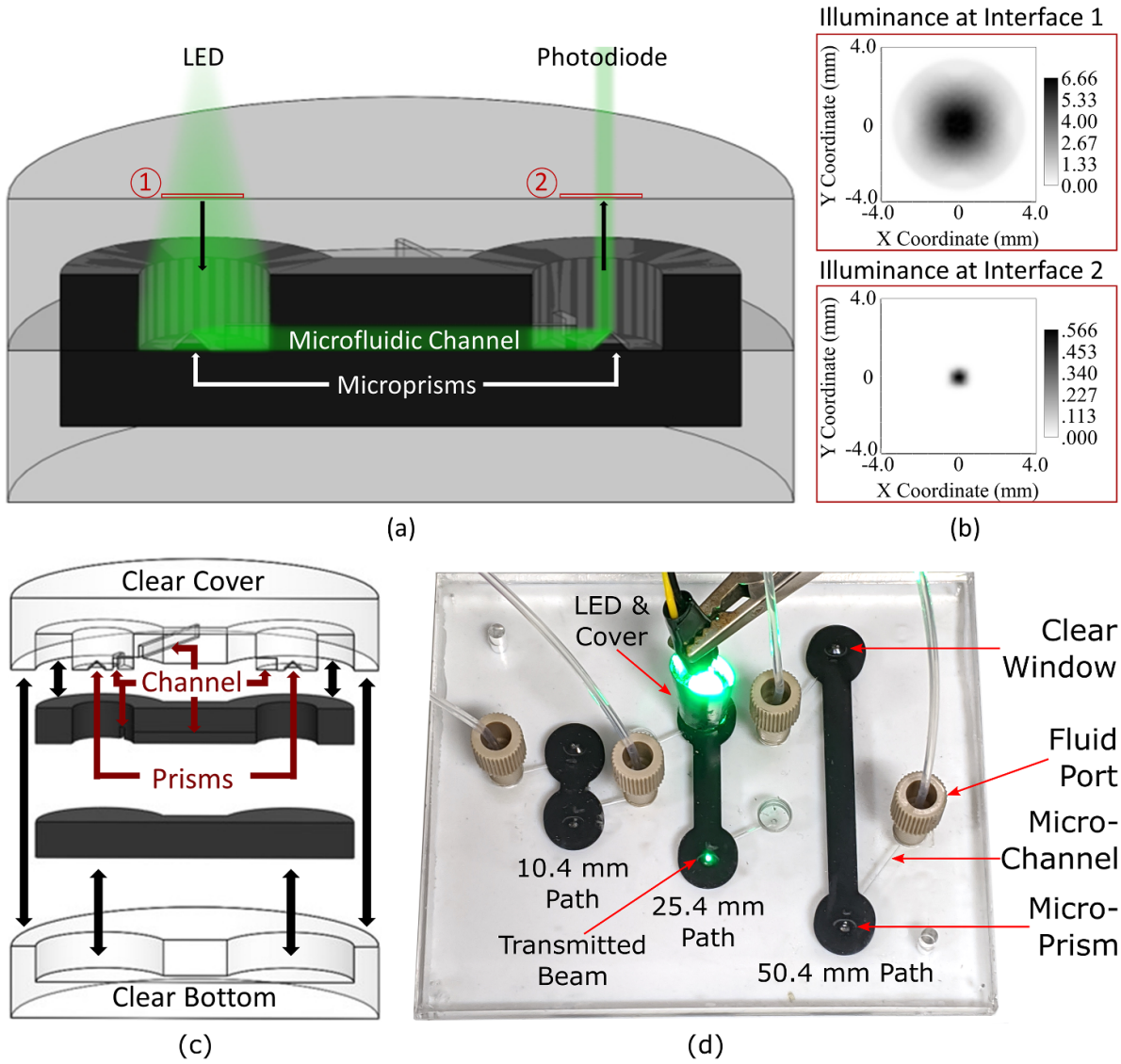

Figure 1. (a) Inlaid microfluidic optical cell concept with a 25.4 mm path length. Uncollimated light sourced from an LED held above the chip passes through a clear window at interface 1. A microprism reflects a portion of this light towards a 25.4 mm long microfluidic channel. Opaque PMMA surrounds the microfluidic channel, blocking non-directional light so that only a focused portion of the reflected beam of light rays pass to the other side through the channel. A second microprism reflects this light out of the chip through another clear window at interface 2 for detection by a photodiode. (b) The luminous flux per unit area (Lumens cm^{-2}) at both highlighted cross-sectional interfaces in (a). (c) CAD exploded view of an inlaid optical cell with a 25.4 mm path length. Features are highlighted with dark-red arrows and assembly with black arrows. (d) Photographed microfluidic chip with multiple inlaid optical cells of varying path length. Light from an LED on the top side of the 25.4 mm long inlaid cell is observed as a green dot at the bottom side, where a photodiode is typically placed. Fluid inlet and outlet ports are also shown.

samples and can produce non-linear correlations if excessively high-concentrations are used. Significantly, the detection sensitivity has a linear dependence on the length of the optical channel: a challenge for microfluidic devices that aim to minimize physical size. This has prompted the use of techniques like cavity ring down spectroscopy [32].

In this work, a light-to-voltage converter is used to measure light intensity. A voltage is measured from the light-to-voltage converter that is proportional to the intensity measured; equation (2) can therefore be rewritten in terms of voltage instead of intensity:

$$A = -\log_{10}\left(\frac{V}{V_0}\right) = \epsilon l c, \tag{3}$$

where V and V_0 are the voltage readings produced by the light-to-voltage converter in response to I and I_0 respectively. These equations, however, assume that all measured light has reached the detector having passed fully through the optical cell and does not account for the detection of any background sources of light (*i.e.* ambient room light, light directly from the light source). Interference from background light must be quantified or otherwise minimized. Equation (3) may be modified to eliminate these external influences and is expressed in

the following equivalent forms:

$$A_{corr} = -\log_{10}\left(\frac{V_{P,S}-V_{bg}}{V_{P,B}-V_{bg}}\right) = A+\log_{10}\left(\frac{1-V_{bg}/V_{P,B}}{1-V_{bg}/V_{P,S}}\right)$$
$$= A+\delta, \quad (\delta \geq 0) \tag{4}$$

where $V_{P,S}$ and $V_{P,B}$ are the photodiode voltage readings when measuring a sample or blank, respectively, and V_{bg} is the voltage measurement of the detector when measuring only the background light. In the final part of equation (4), the corrected absorbance measurement A_{corr} is expressed in terms of the uncorrected absorbance measurement A plus a correction term δ. In practice, δ is always greater than zero when background light is detected; thus, the corrected absorbance measurement is always larger than the uncorrected absorbance measurement. This effect scales with the magnitude of A such that more absorbent samples are more susceptible to the same magnitude of background light than dilute samples. Elaboration on these points, including the derivation of equation (4), may be found in the supplementary material.

Equation (4) requires that, when measuring the light-absorbance of a sample, the amount of background light observed by the detector must be quantified. Measuring the light observed by the detector with the light source turned off provides a good approximation of V_{bg} for use with equation (4), so long as this value remains relatively constant over time. If the amount of background fluctuates with time, the background light must be reassessed for each absorbance measurement. An important consideration of any optical cell, therefore, is to both diminish and minimize fluctuations in the detection of background light.

3. Materials and methods

3.1. Chemistry

All chemicals and reagents were supplied by Fisher Chemical (Springfield Township, NJ, USA), unless otherwise stated. Performance of the absorbance cell was first characterized with two different colors of food dye that had peak absorbances near those of reacted nitrite and phosphate. Red food dye standards were prepared by two-fold serial dilutions of a 0.1% stock, made from dilution of 0.1 ml red food dye (commercial food coloring, Club House Canada) to 100.0 ml with Milli-Q water. Yellow food dye standards were similarly made from diluting a 0.1% stock, made in the same way (commercial food coloring, Club House Canada). Nitrite standards were prepared via stepwise dilution of a 1000 μM stock, mixed from 0.069 g of sodium nitrite ($NaNO_2$, CAS-No: 7632–00-0, EMD Millipore, Germany) and Milli-Q to a total volume of 1 l. Phosphate standards were prepared similarly from a 1000 μM stock, produced by diluting 0.1361 g of potassium phosphate monobasic (KH_2PO_4, BP362-500 LOT 184 646, Fisher Scientific) to 1 l with Milli-Q. Standards were stored in darkness near room temperature between use.

The reagents were prepared so that reagent molecules were in excess of expected nitrite/phosphate ions to ensure color-development is proportional to concentration. The Griess reagent was prepared by combining 0.5 g of sulfanilamide, 5 ml of concentrated HCl, and 0.05 g of NEDD (N-(1-Naphthyl)ethylenediamine dihydrochloride), mixed with Milli-Q to a final volume of 500 ml. Finally, phosphate reagent was prepared similar to Legiret *et al* [29] such that 0.3601 g of ammonium metavanadate and 7.2 g of ammonium molybdate were mixed with 95 ml of concentrated HCl, and brought to a final volume of 1 l with Milli-Q. Constant stirring ensured proper mixing and dissociation of any precipitates formed, and the reagent was allowed to cool to room temperature after the exothermic reaction upon addition of HCl. Chemistry components were of analytical grade, and completed reagents were stored near 4 °C in a dark environment between use.

3.2. Inlay chip fabrication

The fabrication process to create inlaid microfluidic devices is depicted in figure 2. First, from a sheet of opaque or *black* extruded PMMA (9M001, Acrylite, USA), two pieces were cut out to form a top and a bottom 'insert' that are the basis of the inlaid optical channel. The black PMMA inserts were shaped like a dumbbell. The top insert had a straight thin section bounded on either side by rounded ends, $dia._{out} = 11$ mm. The top insert also had inner concentric cylindrical cuts, $dia._{in} = 5$ mm, to allow for light coupling to the prisms. The bottom insert was identical but without the cylindrical cuts to block/absorb light not reflected off the prisms. The top insert for a 10.4 mm inlay cell is shown in figure 2 step 2. The length of each insert depended on the desired length of the optical channel; for example, a 50.4 mm channel insert would measure 50.4 mm between the center of each rounded end. Second, the associated cavities for each insert were machined into a separate sheet of *clear* extruded PMMA (0A000, Acrylite, USA) for each insert to be pressed into. These cavities were of matching dimensions to their corresponding insert except with an added tolerance of 25 μm on all sides—necessary to compensate for microscopic deformities and imprecise milling—so that the inserts fit tightly within the cavities.

In step 3 of figure 2, the inserts and cavities were fused with a solvent, thermal, and pressure process. It was important to achieve a fluid-tight seal between the cavity and the insert such that there were no gaps of empty space upon inlaying. This would ensure uncompromised fluid handling across clear and black sections of the substrate. To achieve a seamless bond between the two plastics, we explored solvent depolymerization then repolymerization at the interface with heat and pressure. With the 25 μm machined tolerance, the bonding method described in Ogilvie *et al* [33] was successfully modified. However, we altered the solvent exposure times as our PMMA was extruded instead of cast. Other approaches to solvent/thermal/pressure bonding of PMMA with absolute ethanol [34], isopropyl alcohol (IPA) [35], or combinations could be employed.

Prior to bonding, a pre-treatment was required for each surface. Pre-treatment included sanding rough edges with a fine-grit paper and light scrubbing with a scotch pad sponge with water and detergent. A toothbrush was used to scrub inside the cavities. Milli-Q rinsing followed, and surfaces

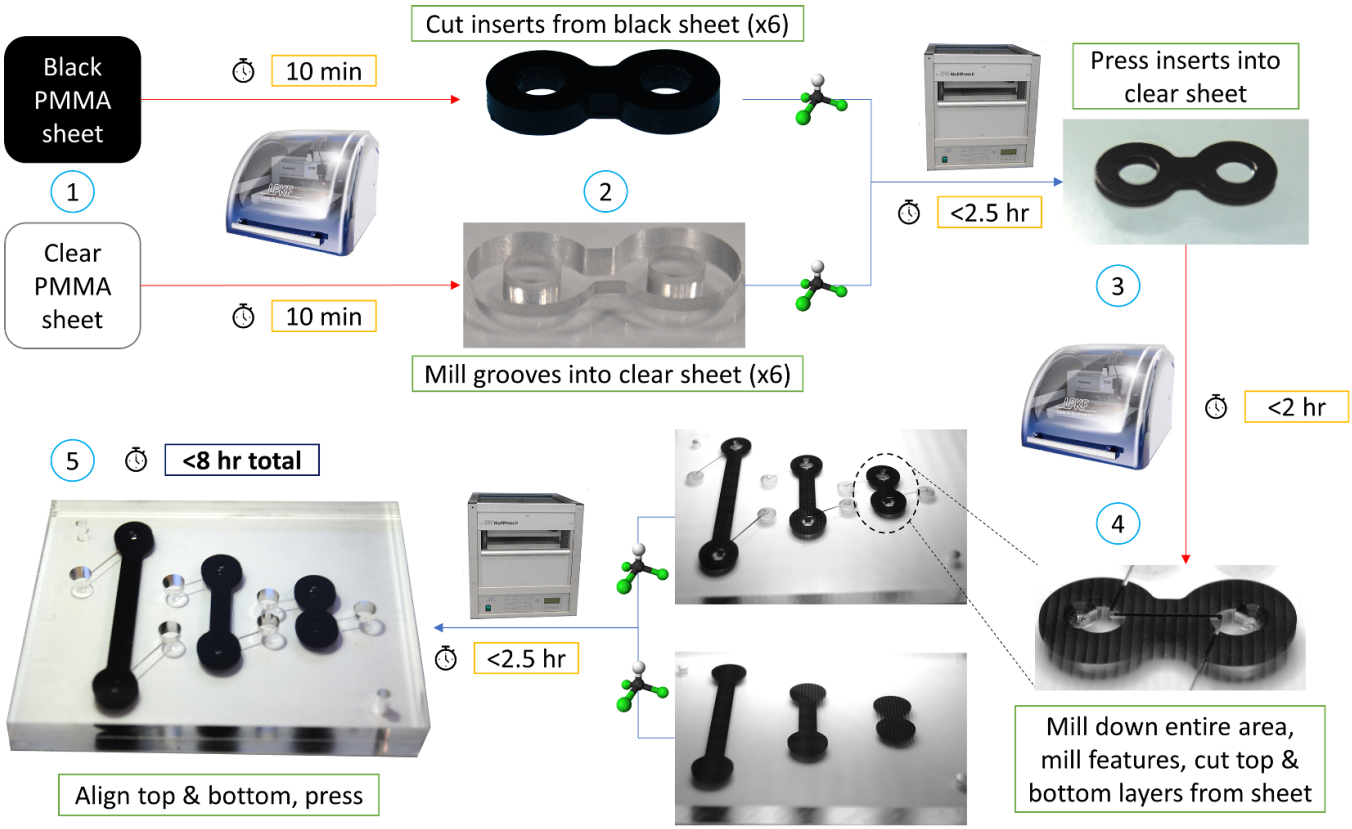

Figure 2. Fabrication process of a microfluidic chip containing three inlaid absorbance cells of varying lengths. Plastic milling occurs via an LPKF S103 Micromill and bonding through pressing chloroform-treated layers within an LPKF Multipress II. Milling times depend on the complexity and size of the design but are listed here as upper-bounds for the depicted inlay optical chip. In step 4, the vertical patterned lines are a result of milling down the area to achieve a smooth surface.

were dried with blasts of compressed air and IPA. After pre-treatment, substrates were ready for bonding. Chloroform (C607-4) was preheated to 30 °C in a sealed container or petri dish. Chloroform-vapor exposure was achieved by suspending each substrate 2 mm above the chloroform liquid line, face down for 45 s. After chloroform exposure, the inserts were quickly slotted into the cavities by hand and manually pressed for approximately half a minute. Next, the clear sheet with the inlay ensemble was pressed for 2.5 h in an LPKF Multipress II set to a pressure of 625 N cm^{-2} and a temperature of 115 °C to approach the glass transition temperature of PMMA as described by Becker and Gärtner in 2000 [36]. After pressing, it was common to observe minor protrusion of the opaque inserts from the sheet. The area that would encompass the entire chip design was milled down by a small amount, approximately 0.3 mm, to restore uniformity. It was found that this step was necessary to prevent delamination when bonding the top and bottom layers together—this preceded step 4.

Step 4 in figure 2 details the creation of alignment holes, fluid channels, vias, syringe ports, and prisms. These were milled into the appropriate spots within the inlaid sheet to realize our microfluidic design. Channels were 400 μm wide and 600 μm deep and were milled into the top layer using a 400 μm mill bit. Each prism was created by cutting into the top layer using a 45-degree end-mill to a depth of 0.8 mm. After bonding the top and bottom layers together, these cuts would create a PMMA-air interface on either end of each optical channel to enable TIR at angles of incidence that exceed θ_c given by equation (1). When milling was complete, two rectangular cuts were made to remove the top and bottom layers from the sheet. Both layers were left overnight on a hot plate set to 85 °C to release residual stress and/or solvent vapor trapped within the inlay. The top and bottom layers were then bound together using the same bonding and pressing parameters as above with 45 s chloroform-vapor exposure time; however, at 85 °C instead of 115 °C. Corresponding holes in both layers were used for alignment with cylindrical metal dowels of length greater than the thickness of one layer but less than the combined thicknesses of both. Assembly of inlay chip was complete after this point, step 5 in figure 2. The microfluidic chip photographed in figure 2 was used to validate the performance of our optical cell.

3.3. *Optical cell testing apparatus*

Two LEDs centered at $\lambda_1 = 527$ nm (Cree C503B-GAN-CB0F0791-ND, FWHM = 15 nm) and $\lambda_2 = 380$ nm (Superbrightleds RL5-UV0315-380, FWHM = 12 nm) were used to perform absorbance spectroscopy on reacted nitrite and phosphate samples—and their corresponding food dye samples—respectively with detection by a Digikey TSL257 High-Sensitivity Light-to-Voltage Converter (photodiode). A

voltage is produced by the photodiode proportional to the intensity of light measured by the photodiode; thus, these voltages measurements can be used with equation (4) to calculate light-absorbance. A custom-built LED driver allowed adjustment of LED intensity while maintaining constant current. The voltage output of the photodiode was connected to a B&K Precision 5491B bench multimeter with 10^{-7} V precision. The sampling rate was set to its maximum, and each measurement along with their date and time was recorded on a personal laptop connected to the multimeter via USB.

LED intensity was adjusted with Milli-Q in the channel to maximize light detection without saturating the photodiode. Since sources and detectors were held externally to the chip, a single set of optical components (LED and photodiode) were used for all three path lengths and the entire testing process. To inspect a sample using one of the three optical cells, the relevant LED was held in place directly above a prism using a metal clamp and a photodiode was held face-down above the prism on the other end. Swapping between each of the three optical cells or changing LEDs between test series was simple due to the decoupled components: a useful advantage of this optical system. A custom opaque enclosure was placed over the entire testing apparatus to minimize background light reception.

Fluid injection for the red food dye and nitrite tests was performed manually with syringes. Yellow food dye and phosphate tests were completely automated using an off-the-shelf Cavro XC syringe pump (PN 20 740 556-C, Tecan Systems, San Jose, CA) and a Vici Cheminert C65Z 10-port selector valve (Model No. C65-3710IA, Valco Instruments Co. Inc. Houston TX). Each of the four inspected species were analyzed using all three optical channels a total of three times each. At the start, end, and between each sample, Milli-Q was pumped through the channel to flush the system and reduce sample–sample crosstalk. This also served as a blank measurement for all but the phosphate tests wherein a 1:1 volumetric mix of Milli-Q and reagent was used instead to serve as the blank since the inherent color of the reagent itself was a light-yellow. All samples and blanks were analyzed for a period of five minutes; the average voltage over the final minute was used to determine absorbance. Nitrite samples were analyzed immediately following reaction with the Griess reagent whereas phosphate samples were premixed several hours before analysis permitting complete reaction. Finally, at the beginning and end of every test, a measurement of the background light was taken over a minute interval. These values were very small relative to the blank reading and were averaged together for use with equation (4) to account for background light for each light-absorbance measurement taken through the test.

4. Results and discussion

4.1. Food dye calibration and nutrient detection

Figure 3 below depicts the raw data produced by light-absorbance experiments of yellow food dye, nitrite, and phosphate through our 10.4 mm inlaid cell. The performance of our inlaid optical cell design was first evaluated with stable food dyes before analyzing nutrient samples. Food dye calibration tests are a standard benchmark towards proving robust, accurate, and reliable light-absorbance measurements of an optical cell [37]. There are several external factors that may influence the light-absorbance of a reacted nutrient sample with reagent. These include sample degradation, reagent degradation, incorrect sample or reagent make-up, and the kinetics of the reaction between nutrient and reagent. In the case where samples do not produce the expected results—i.e. conforming to the Beer–Lambert law given by equation (2)—it is difficult to determine if the design of the optical cell is at fault or the analyzed samples themselves. Red dye was chosen to mimic reacted nitrite due to its absorbance spectrum with a strong absorbance peak in the same 540 nm region. Using the 527 nm LED, light-absorbance measurements were taken through red dye samples ranging from 0.0016% to 0.05% (v/v). Similarly, yellow food dye was chosen due to mimic reacted phosphate where the peak absorbance spectrum was 375 nm and inspected using the 380 nm LED A range of yellow dye was tested between 0.0063%—0.1% (v/v). After successful food dye experiments, nitrite samples were reacted with the Griess reagent and analyzed. Nitrite standards ranged in concentration from 0.1 μM to 100 μM and were measured using the 527 nm LED, after mixing in a 1:1 volumetric ratio with reagent. Therefore, the final concentration of each analyzed sample was half that of the standard. Finally, phosphate standards between 0.1 μM—50 μM were reacted with phosphate reagent and were analyzed using the 380 nm LED.

Figure 3(a) shows 5 concentrations of yellow food dye analyzed a total of three times through a 10.4 mm long inlaid optical cell; each series produced consistent results. Milli-Q blanks preceded each sample as described in section 3.3. Near the 67-minute mark, a temporary drop in voltage can be observed: this was likely the result of an air bubble in the measurement channel during stopped flow. Additional sample was injected into the cell to displace the bubble, which restored the expected voltage reading as seen before and after this drop. Finally, at the end of the trial, a measurement was taken to quantify the background light by turning off the LED light source. This is labelled as 'Dark Ref.' on figure 3(a) and was consistently 7 mV $\pm$ 1 mV throughout experiments in this manuscript, highlighting the effectiveness of our design in minimizing background light contributions.

Figure 3(b) depicts the results of a nitrite experiment performed using 12 standards with Milli-Q blanks between them and with concentrations labelled on each plateau. Nitrite samples were analyzed immediately after mixing with the Griess reagent. The reaction kinetics can be observed by the color-development of each reacting sample; i.e. voltage over time. Initially, there was a rapid drop in voltage at the beginning of each reaction followed by a gradual decrease until a plateau was reached. The lower-concentration nitrite samples, less than 5 μM, appear to have completely reacted almost immediately, attaining 95% of the plateau value within 15 s. The higher-concentration nitrite samples, near 50 μM, took longer to react and required 44 s to attain 95% of the plateau value.

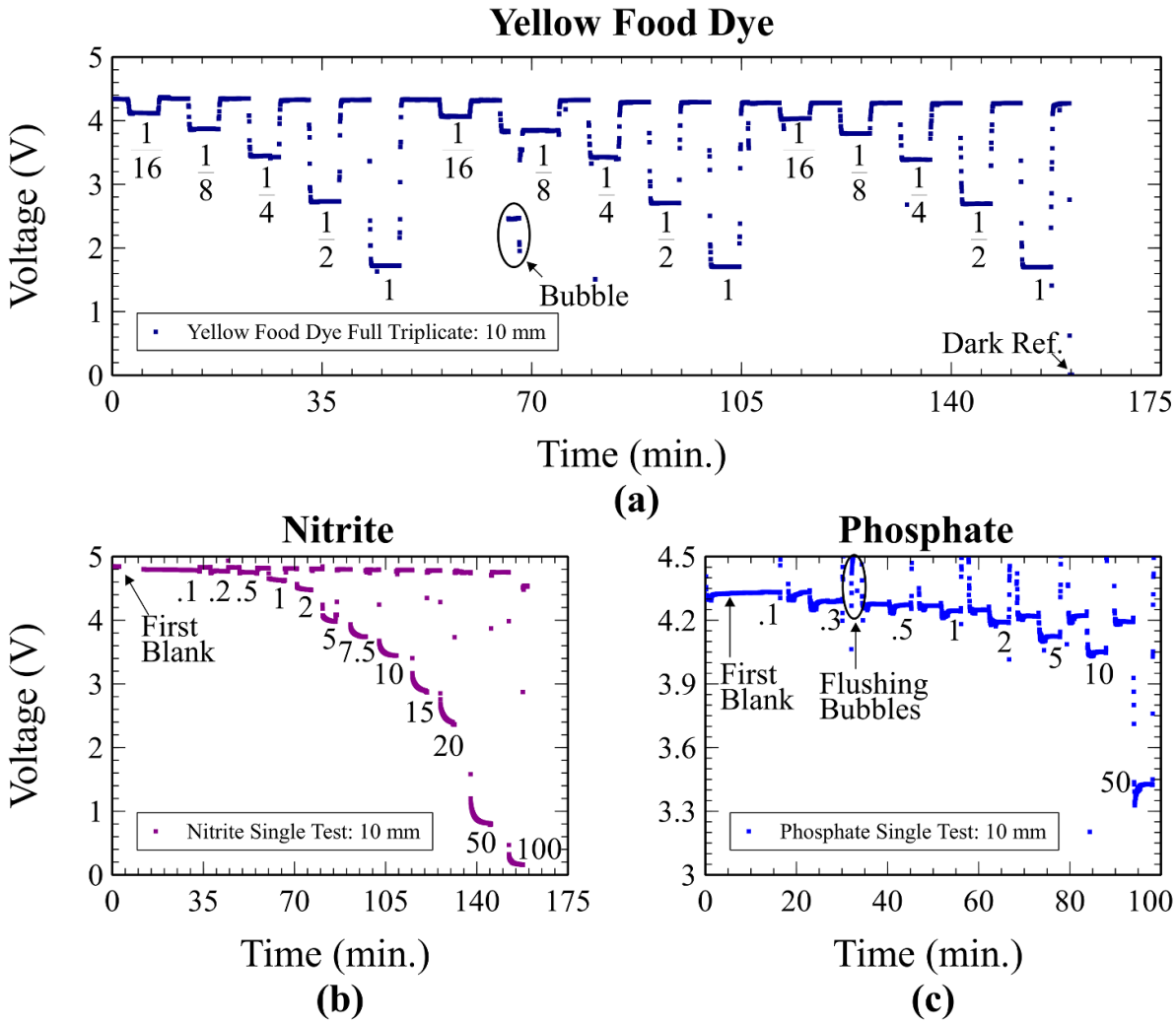

Figure 3. Raw photodiode voltage vs. time of typical (a) yellow food dye, (b) nitrite, and (c) phosphate experiments through the 10.4 mm inlaid optical cell. The dye plot in (a) depicts an entire triplicate with labels normalized to the highest concentration sample: 0.1%. The nitrite and phosphate plots depict a single trial within a triplicate, and labels indicate the concentration of the associated standard before mixing with reagent. Blanks are analyzed between successive samples. The final minute of voltage data obtained from each blank or sample measurement was averaged together to obtain either $V_{P,B}$ or $V_{P,S}$ for use with equation (4).

Figure 3(c) shows the results of a phosphate experiment performed with 8 standards. Here, the blank was a 1:1 volumetric mix of Milli-Q and phosphate reagent, which was injected between standards. The sequence of injection was blank, sample and then pure Milli-Q water. The Milli-Q water flush was used as a precaution to minimize crosstalk between standards. The Milli-Q flush can be observed in figure 3(c) as sudden voltage spikes which saturate the photodiode since the pure Milli-Q is colorless compared to the blank (LED intensity is set based on blank). Also highlighted in figure 3(c) is an instance where air bubbles momentarily entered the measurement channel: this was remedied with further pumping but produced a minor offset to further voltage data (corrected-for in each absorbance measurement by the blank). For the phosphate experiments, samples were fully reacted prior to injection into the optical cell. The yellow method has similar development times to the Griess method: 1–5 min [29]. We chose to pre-react the phosphate to benchmark stable nutrient samples; hence, the relatively constant voltage plateaus. In figure 3(c), we observe a minor drift of the blank voltage, decreasing 100 mV over the 6000 s duration of the experiment, which was less than a 2% drop over 1.5 h. It is interesting to note that the yellow dye experiment in figure 3(a) also drifted down, 70 mV over 6000 s, but this is less visible because of the *y*-axis scale. The drift was repeatably observed for the phosphate and yellow dye measurements, indicating it is not the phosphate chemistry. The gradual voltage decrease between blanks is most likely due to UV–fluid interaction or ageing of the PMMA plastic through prolonged intense UV-exposure.

Figures 4(a)–(b) depict the expected linear relationships between sample concentration and absorbance for red food dye and reacted nitrite samples. Light-absorbance of each species was characterized using three inlaid microfluidic cells with optical path lengths of 10.4 mm, 25.4 mm, and 50.4 mm, labelled as 10 mm, 25 mm, and 50 mm in the legend, respectively. In practice, shorter optical channels are used to detect highly concentrated samples, but they are less sensitive (smaller slope in Beer–Lambert law). Longer channels are used for

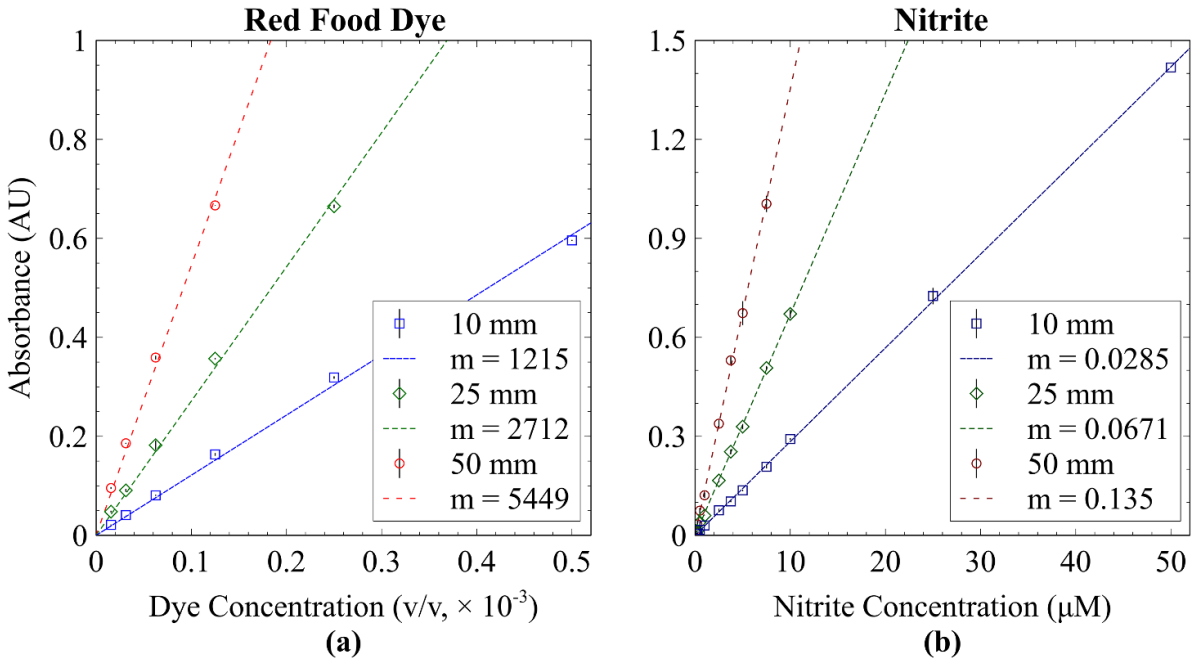

Figure 4. Absorbance versus concentration for (a) red food dye and for (b) reacted nitrite samples. The nitrite concentration represents the final concentration in the flow cell after mixing with Griess reagent. The absorbance of each sample concentration is the average from three experiments with vertical error bars representing standard deviations. Linear fits are shown with $R^2 > 0.99$, as expected by equation (2).

detecting small variations and low concentrations but are also more susceptible to noise from bubbles and particulates. Each calibration curve depicted in figure 4 represents the average of three independent experiments, except the 10.4 mm nitrite series where only two trials were performed. Equation (4) was used to calculate the absorbance of each sample from their associated photodiode readings, referenced to the voltage of the prior blank and the voltage produced from background light. Linear trendlines with forced-zero intercepts were fit to each series with strong agreement to the data.

In figure 4(a), each optical cell (10.4, 25.4, and 50.4 mm) was evaluated with four to six different concentrations depending on the path length. The 10 mm path length was evaluated with six samples and maintained linear results consistent with equation (2), even for the most concentrated samples. The 25 mm path length cell showed a linear relationship for the first five samples. The 50 mm path length showed a linear relationship for the first four samples. Figure 4(b) depicts the absorbance of various concentrations of reacted nitrite samples. The final concentration of nitrite after mixing with reagent is used to reflect the true concentration in the absorbance cell. All twelve standards were analyzed using the 10 mm cell; whereas, the least-concentrated ten and nine standards were analyzed with the 25 mm and 50 mm cells, respectively. For the concentrations tested, we conclude that our inlaid optical absorbance cells showed excellent linear relationships.

Figures 5(a)–(b) plot absorbance versus concentration for yellow food dye and reacted phosphate samples. Figure 5(a) depicts five yellow food dye samples analyzed with the 10 mm and 25 mm optical path lengths, and four samples analyzed on the 50 mm optical path length. All three data sets showed excellent linear fits for their entire concentration range. Similarly, in figure 5(b), the absorbance for all eight phosphate standards show the expected linear relationships.

Table 1 shows experimentally determined attenuation coefficients for both dyes, nitrite, and phosphate for all three path lengths tested. These quantities are specific to the inspection light wavelengths, i.e. 527 nm for red food dye and reacted nitrite, and 380 nm for yellow food dye and reacted phosphate. An average attenuation coefficient of nitrite was found to be $\epsilon_{NO_2^-} = 0.0269\ (\mu\text{M cm})^{-1}$. The value is in agreement with literature values for $\epsilon_{NO_2^-}$, which range between 0.014–0.039 $(\mu\text{M cm})^{-1}$ [8, 9, 38, 39] for Griess reagent and light centered near 525 nm. Similarly, an average attenuation coefficient for phosphate was found to be $\epsilon_{PO_4^{3-}} = 0.00335\ (\mu\text{M cm})^{-1}$. This value is also in agreement with literature values that range between 0.0036–0.00503 $(\mu\text{M cm})^{-1}$ [28, 29, 40] for the yellow method using light centered near 380 nm. For all three path lengths, the attenuation coefficients determined for nitrite and phosphate using these color-developing techniques agree with the literature which further supports the performance of this novel optical cell.

4.2. Detection limits

The LOD can be a useful measure of a sensing apparatus' measuring capabilities and is specific to each species measured. The resolution of the system can be quantified by measuring the average noise of *n* blanks. The LOD for both nitrite and phosphate was evaluated for each optical path length using the standard triple-sigma literature method [9, 29, 42], which uses three-times the blank baseline noise as a reference. A blank value of 4.80 V—just below photodiode

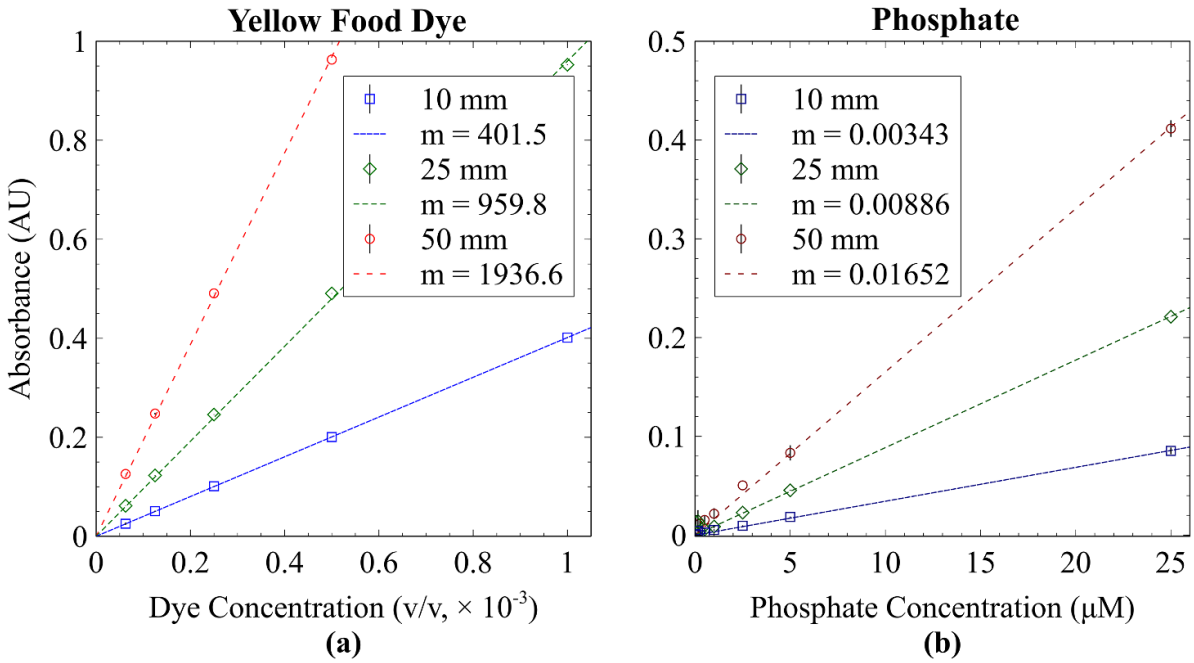

Figure 5. Absorbance versus concentration for (a) yellow food dye and for (b) reacted phosphate samples. The absorbance of each sample concentration is the average from three experiments with vertical error bars representing standard deviations. Linear fits are shown with $R^2 > 0.99$, as expected by equation (2).

Table 1. Experimentally obtained attenuation coefficients ϵ for red dye, nitrite, yellow dye, and phosphate for each optical path length. $\bar{\epsilon}$ is the average with standard deviation. σ_{dye} is volume concentration such that $\sigma_{dye} = v_{dye}/v_{solution}$. Data shown with precision relative to their error (standard deviation of all repeated trials) following [41].

	Red Food Dye		Nitrite		Yellow Food Dye		Phosphate	
l (mm)	$\epsilon_{RFD}(\sigma_{dye}\ cm)^{-1}$	$\bar{\epsilon}$	$\epsilon_{NO_2^-}\ (\mu M\ cm)^{-1}$	$\bar{\epsilon}$	$\epsilon\ (\sigma_{dye}\ cm)^{-1}$	$\bar{\epsilon}$	$\epsilon_{PO_4^{3-}}\ (\mu M\ cm)^{-1}$	$\bar{\epsilon}$
10.4	1168	1100	0.0273	0.0269	386.1	383 ± 4	0.00330	0.00335
25.4	1068	±	0.0264	±	377.9	±	0.00349	±
50.4	1081	50	0.027	0.0005	384.24	4	0.00328	0.00012

saturation—was chosen to convert each LOD from voltage to absorbance units. The absorbances were then converted to concentrations by dividing by the respective slope for each species. Our results are summarized in table 2 below.

These detection limits are consistent with those found in the literature; for example, Sieben *et al* in 2010 had an LOD of 14 nM for nitrite using a 25 mm optical path, and Legiret *et al* in 2013 had an LOD of 52 nM using a 25 mm path and the yellow phosphate method. A notable trend is that, among each path length, the average noise of the nitrite blanks is greater than those of the phosphate blanks: this may be a consequence of the manual sample injection method used for the nitrite samples. A benefit of automated sample injection is more consistent injection flow rates between each sample. Although the LODs are 6 nM and 40 nM, the limit-of-quantification (LOQ) would be more appropriate as a lower sensing bound when these inlaid flow cells are integrated into marine sensors. Typically, the LOQ is ten times the blank noise, and in our case would be 20 nM and 150 nM for nitrite and phosphate, respectively. Our observations confirm this with the standards evaluated in this study.

4.3. Sensor integration

A lab-on-chip system containing two inlaid optical cells ($l = 10$, 25 mm) and 4 microfluidic check-valves was fabricated to validate our approach with more complicated integrations. In a deployment scenario, having a second optical channel with a shorter path length can be beneficial when entering highly concentrated nutrient-rich zones but has lower sensitivity to minor concentration fluctuations. Figure 6(a) depicts the fluidic schematic of the lab-on-chip. Microfluidic flap-based check valves were integrated within the chip to govern the direction of fluid flow while pumping. The sample intake port of the sensor (SP) was connected via tubing to the output of a 10-port selector valve (not shown). The selector valve was used to sample either one of eight nitrite standards or Milli-Q. The reagent intake tube (GR) was connected to a bag containing freshly-prepared Griess reagent. Both sample and reagent channels joined at a Y-junction after which the two fluids mixed via diffusion in a microfluidic mixing chamber. Two inlaid optical cells with 25 mm and 10 mm path lengths were then used to capture any colour-development via

Table 2. LODs for nitrite and phosphate for each optical path length; n represents the number of blanks analyzed, each over five minutes. The slopes depicted in figure 4(b) and figure 5(b) are used to convert absorbance to concentration for each path length.

	Nitrite				Phosphate			
l (mm)	n	Avg. Blank Noise (mV)	LOD (mAU)	LOD (nM)	n	Avg. Blank Noise (mV)	LOD (mAU)	LOD (nM)
10.4	23	3 ± 2	0.9 ± 0.6	30 ± 20	24	1.3 ± 0.9	0.3 ± 0.3	100 ± 80
25.4	31	4 ± 5	1.0 ± 1.3	14 ± 19	20	2 ± 2	0.6 ± 0.6	60 ± 70
50.4	22	3 ± 4	0.7 ± 1.0	6 ± 8	23	2.7 ± 1.8	0.7 ± 0.5	40 ± 30

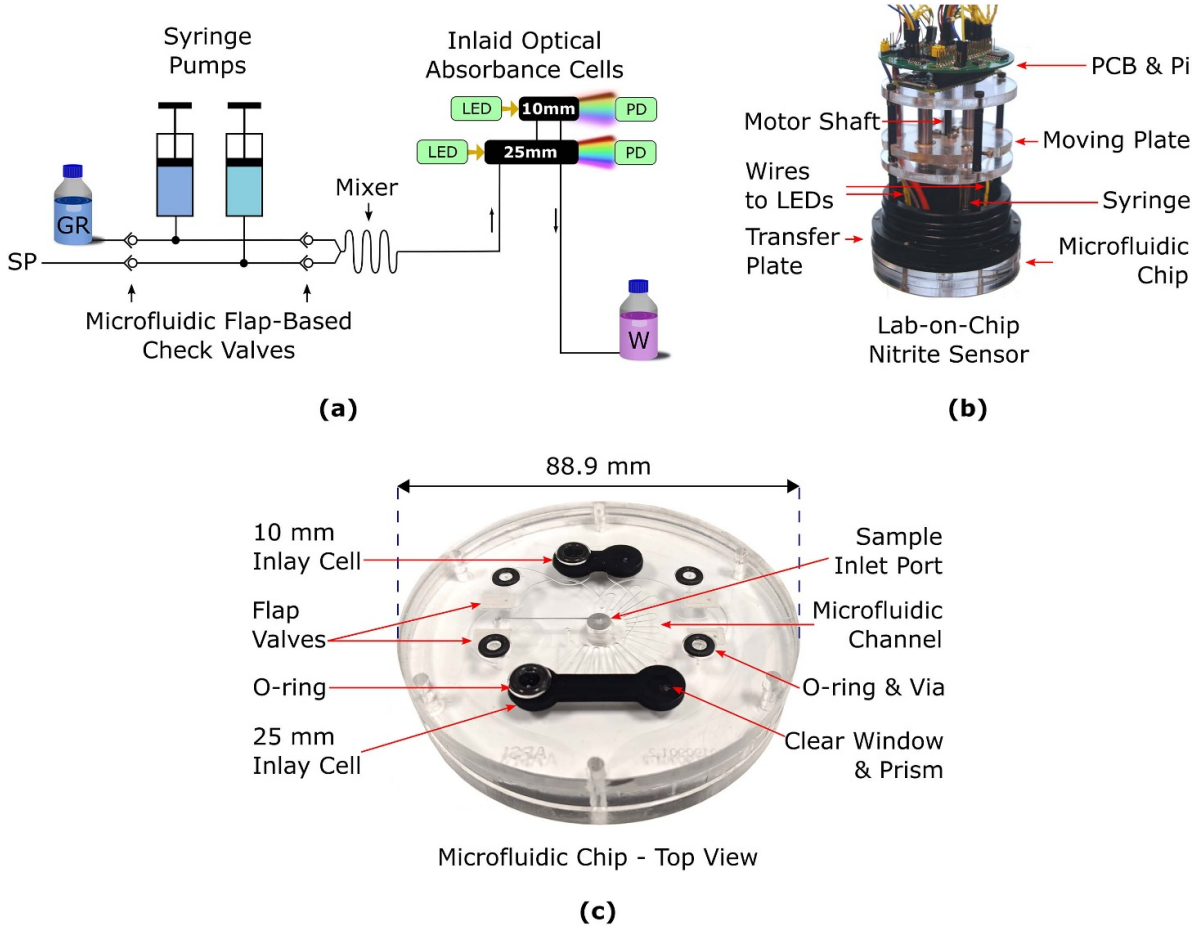

Figure 6. (a) Flow schematic for a lab-on-chip nitrite sensor using inlaid optical cells. SP refers to the sample intake port of the chip and GR refers to the Griess reagent intake. Sample and reagent join at a Y-junction and mix via diffusion in a microfluidic mixing chamber. Developing samples are analyzed using two inlaid optical cells before dispensing to a waste container (W in the diagram). (b) Lab-on-chip nitrite sensor photograph. (c) Photograph of the microfluidic chip with labelled features. The chip has a diameter of 88.9 mm and a thickness of 16 mm.

light-absorbance. To acquire measurements, flow was stopped for 5 min and the voltage for both optical channels was recorded. The last 30 s of each measurement were averaged to acquire the voltage used for absorbance and concentration calculations. After this period, flow resumed, and mixed samples were dispensed from the chip to a waste container.

Figure 6(b) shows the physical implementation of the system. Two 250 μl syringes—one for sample and one for reagent—were connected to the chip and were responsible for pumping. A single stepper motor was utilized for actuation of both syringes such that both were pulled or pushed simultaneously. The two syringes were screwed into the top of the transfer plate and O-rings between the chip and plate established a fluidic seal via compression. Optical components were also held in slots machined into the transfer plate to maintain alignment with the chip. A custom PCB integrated the electronics to handle stepper motor control (pumping), hall effect sensing (plate position), analog signal processing, data storage and interfacing to a Raspberry Pi Zero, located at the top of the sensor. Custom firmware was also created to automate the sampling process mentioned above. The final lab-on-chip sensor is shown in figure 6(c).

The results of the three lab-on-chip nitrite sensor tests are shown in figure 7. Eight nitrite standards between 0.1–20 μM were analyzed from low to high concentration using both optical cells. Blank measurements were taken before each

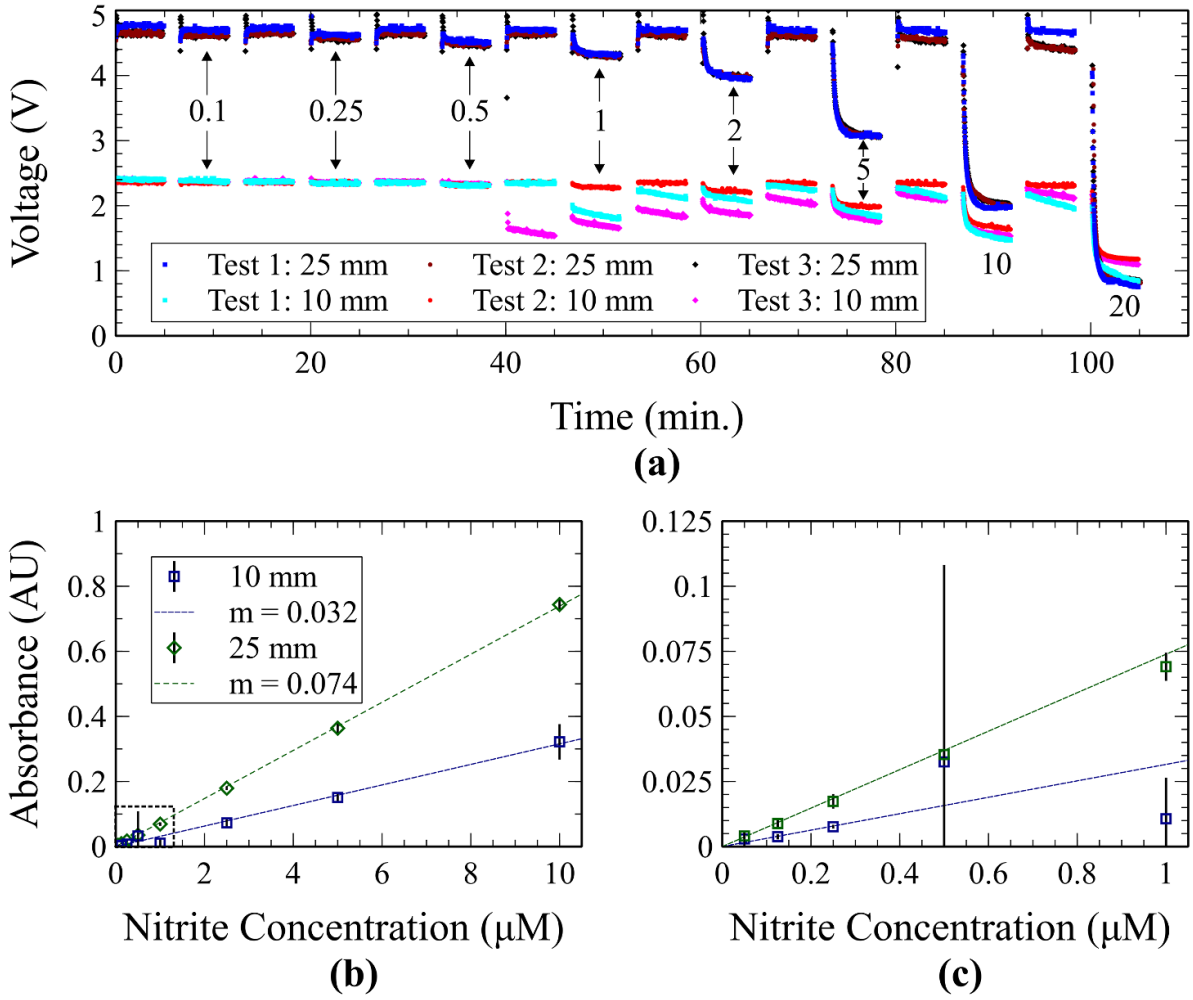

Figure 7. Results from a benchtop calibration experiment of the automated lab-on-chip nitrite sensor. (a) Raw photodiode voltage measurements taken during each of the three tests from both photodiodes. Times are determined from the beginning of each test, starting when pumping of the first blank begins. Labels indicate the concentration of the standard injected through the sample port. (b), (c) Light-absorbance measurements plotted against sample concentration assuming a 1:1 mixing ratio between standard and reagent. Blue data points are averaged absorbance measurements taken using the 10 mm optical cell and green with the 25 mm cell. Each average is comprised of three independent measurements, each referenced to a blank, taken over the course of three individual tests but using the same batch of standards and reagent. Error bars represent standard deviations; the large error bar seen at 0.5 μM corresponds to the reading of the 0.5 μM sample with the 10 mm path. (c) Nitrite absorbance data for low concentrations—dashed box in (b).

sample, comprised of both Milli-Q and Griess reagent in the same volumetric ratio. One complete test consisted of 8 nitrite and 8 blank measurements for a total of 16 measurements per optical channel. Three of these tests were performed to assess measurement error and to quantify the reliability of the completely integrated lab-on-chip system. The same standards and reagent were used for all three tests, and all three tests were conducted within a two-day period.

Figure 7(a) shows a time series of the raw photodiode output voltage produced by the photodiodes measuring each optical channel. Gaps in the data after each blank and sample measurements are during pumping during which measurements of the background light were taken by turning both LEDs off—data not shown. Lower voltages are observed in each 10 mm test—approximately half the normal voltage reading when measuring blanks—due to misalignment between LED and prism. The slot in the transfer plate holding that LED was machined slightly offset to the window of the optical cell which prevented proper light coupling. This can easily be fixed in future designs by modifying the machining of the transfer plate.

The 25 mm long optical cell produced expected and repeatable results for each of the three tests. The dark blue, maroon, and black data points in figure 7(a) depict the voltage time-series of each of the three 25 mm tests and are self-consistent apart from the final blank reading. The drop in the final blank measurement observed in tests two and three is indicative of crosstalk from the previous sample: this could be remedied with more comprehensive flushing between samples. Small vertical error bars in figures 7(b) and (c), calculated as the standard deviation of each repeated measurement, confirm highly consistent results over the whole 0.1–20 μM domain. Figure 7(c) better represents the data for lower concentrations, showing close conformity between these data points and the

overall trendline. The LOD of the 25 mm path was determined following section 4.2 to be 39 ± 8 nM. The increased measurement noise from the photodiode led to a slightly worse LOD than that observed in the isolation tests where a high precision multimeter was used.

The 10 mm long optical cell produced unexpected results, as shown by the time-series data in figure 7(a). The three tests represented by the cyan, red, and magenta data points were not consistent. Test 2 produced the expected linear relationship over the entire concentration range, with a fit of $A = 0.029$ (NO_2^-) and an R^2 of 0.9995. Tests 1 and 3 produced data in excellent agreement with test 2 for the first three samples of 0.1, 0.25 and 0.5 μM. However, tests 1 and 3 were subject to measurement errors for the next three samples, which included 1, 2 and 5 μM samples. For example, in test 3 there is an unexpected and large drop in the voltage data. The drop in voltage persisted over the next three measurements but trended back toward the expected baseline. We attribute this to a bubble being trapped in the measurement cell that was gradually dislodged. The inlaid optical cell design, like most fluidic systems, is prone to bubble measurement errors; however, less so than wide channel designs. To detect and account for these errors, onboard standards should be carried for autonomous *in situ* deployments. After the bubble was cleared from the short path length cell, the 10 and 20 μM samples measured consistently for tests 1, 2 and 3.

The correlation slope of the 25 mm and 10 mm absorbance vs. concentration curve is approximately 10% higher than those determined in section 4.1, figure 4(b). We attribute this offset to biased mixing between reagent and sample. Ideally, both sample and reagent were pumping in equal volumes since they both actuated together. However, our check-valves may have had some degree of backflow, altering the mixing ratio. If we assume the sample-to-reagent volumetric ratio is 55:45, then our slopes match section 4.1. This indicates the reagent valve had a backflow of approximately 5%. Future work will focus on improving check-valve performance and to attain an expected 1:1 ratio. However, on-board standards would allow us to apply the corrected linear relationship, even if the mixing ratio is non-ideal. We conclude that, over the tested concentrations, the lab-on-chip sensor based on our inlaid optical cell produced highly repeatable and accurate nitrite detection.

5. Conclusion

The fabrication process of a novel optical absorbance cell is presented in which transparent and opaque PMMA are combined to create an isolated absorbance cell within a microfluidic chip. Optical components are decoupled from the chip using integrated v-groove prisms to improve manufacturability. Light-absorbance measurements were performed using channels 400 μm wide and 600 μm deep. Optical path lengths were 10.4 mm, 25.4 mm, and 50.4 mm, for total sample volumes ranging between 2.5 and 12 μl. With optimization, we can readily achieve 100–200 μm channels and thus attain nanoliters per measurement. Samples of varying food dye concentration as well as nitrite and phosphate samples were used to verify the measuring capabilities of our novel inlaid approach. Excellent linear relationships were observed between absorbance and concentration for all tested samples. Going forward, the inlaid method of combining multiple types of PMMA will form the basis of many *in situ* marine sensors for high-performance colorimetric measurements. Here, a complete lab-on-chip nitrite sensor was demonstrated that used two inlaid optical cells to measure light-absorbance with accurate and reproducible nitrite detection from 50 nM to 10 μM. Beyond absorbance measurements, PMMA of various colors could be utilized to implement filters for optical techniques like fluorescence spectroscopy or viewing ports to capture light from predetermined scattering angles. The 'inlaid' approach will find broad applicability for performing optical measurements on lab-on-chip devices.

Acknowledgment

Acknowledgments are made to Mitchell Szeto for partial data collection.

Conflict of interest

The authors declare no conflict of interest. The funders had no role in the design of the study; in the collection, analyses, or interpretation of data; in the writing of the manuscript, or in the decision to publish the results.

Notes on contributors

E L and S M conceived the inlay design and fabricated the microfluidic chips; E L performed the experimental work and data analysis; S M performed optics simulations; E L, S M, J C, and B M fabricated the lab-on-chip sensor with testing by E L, J C, and B M; J C automated the benchtop testing apparatus and wrote software; E L wrote the original draft, E L and V S reviewed and edited the paper; V S acquired funding and supervised the project.

Funding

Gratitude is expressed towards the Marine Environmental Observation, Prediction and Response Network (MEOPAR), the Natural Sciences and Engineering Research Council (NSERC), the Canada First Research Excellence Fund (CFREF) through the Ocean Frontier Institute (OFI), Innovacorp Early Stage Commercialization Fund (ESCF), and RBR Ltd for funding.

ORCID iD

Vincent J Sieben https://orcid.org/0000-0002-6289-9440

References

[1] Paiè P, Martínez Vázquez R, Osellame R, Bragheri F and Bassi A 2018 Microfluidic based optical microscopes on chip *Cytometry* A **93** 987–96

[2] Jeon H, Kim S and Lim G 2018 Electrical force-based continuous cell lysis and sample separation techniques for development of integrated microfluidic cell analysis system: a review *Microelectron. Eng.* **198** 55–72 Oct

[3] Gross E, Durant H, Hipp K and Lai R 2017 electrochemiluminescence detection in paper-based and other inexpensive microfluidic devices *Chem. Electro. Chem.* **4** 1594–603

[4] Tycova A, Přikryl J and Foret F 2017 Recent strategies toward microfluidic-based surface-enhanced Raman spectroscopy *Electrophoresis* **38** 1977–87

[5] Weibel D B and Whitesides G M 2006 Applications of microfluidics in chemical biology *Curr. Opin. Chem. Biol.* **10** 584–91

[6] Dhar B C and Lee N Y 2018 Lab-on-a-chip technology for environmental monitoring of microorganisms *Bio. Chip. J.* **12** 173–83

[7] Antweiler R C, Patton C J and Taylor H E 1996 Automated, colorimetric methods for determination of nitrate plus nitrite, nitrite, ammonium and orthophosphate ions in natural water samples *U.S. Geological Survey* Open-File Report 93–638

[8] Beaton A D, Cardwell C L, Thomas R S, Sieben V J, Legiret F-E, Waugh E M, Statham P J, Mowlem M C and Morgan H 2012 Lab-on-chip measurement of nitrate and nitrite for in situ analysis of natural waters *Environ. Sci. Technol.* **46** 9548–56

[9] Sieben V J, Floquet C F A, Ogilvie I R G, Mowlem M C and Morgan H 2010 Microfluidic colourimetric chemical analysis system: application to nitrite detection *Anal. Methods* **2** 484–91

[10] Ahn J-H, Jo K and Hahn J 2015 Standard addition/absorption detection microfluidic system for salt error-free nitrite determination *Anal. Chim. Acta.* **886** 114–22 Jul

[11] Khanfar M F, Al-Faqheri W and Al-Halhouli A 2017 Low cost lab on chip for the colorimetric detection of nitrate in mineral water products *Sensors* **17** 2345

[12] González P, Pérez N and Knochen M 2016 Low cost analyzer for the determination of phosphorus based on open-source hardware and pulsed flows *Quím. Nova* **39** 305–9

[13] Duffy G, Maguire I, Heery B, Nwankire C, Ducrée J and Regan F 2017 PhosphaSense: a fully integrated, portable lab-on-a-disc device for phosphate determination in water *Sensors Actuators* B **246** 1085–91

[14] Grand M M, Clinton-Bailey G S, Beaton A D, Schaap A M, Johengen T H, Tamburri M N, Connelly D P, Mowlem M C and Achterberg E P 2017 A lab-on-chip phosphate analyzer for long-term in situ monitoring at fixed observatories: optimization and performance evaluation in estuarine and oligotrophic coastal waters *Front. Mar. Sci.* **4** 255

[15] Chen Y *et al* 2018 Toward an in situ phosphate sensor in natural waters using a microfluidic flow loop analyzer *J. Electrochem. Soc.* **165** B737–B745

[16] Yan J-C *et al* 2019 Development of a portable setup using a miniaturized and high precision colorimeter for the estimation of phosphate in natural water *Anal. Chim. Acta.* **1058** 70–79

[17] Ozhikandathil J, Badilescu S and Packirisamy M 2018 Polymer composite optically integrated lab on chip for the detection of ammonia *J. Electrochem. Soc.* **165** B3078–B3083

[18] Li P *et al* 2019 High-frequency underway analysis of ammonium in coastal waters using an integrated syringe-pump-based environmental-water analyzer (iSEA) *Talanta* **195** 638–46

[19] Duffy G, Maguire I, Heery B, Gers P, Ducrée J and Regan F 2018 ChromiSense: A colourimetric lab-on-a-disc sensor for chromium speciation in water *Talanta* **178** 392–9

[20] Devi V S A and Reddy V K 2012 Spectrophotometric determination of iron(II) and cobalt(II) by direct, derivative, and simultaneous methods using 2-hydroxy-1-naphtha ldehyde-p-hydroxybenzoichydrazone *Int. J. Anal. Chem.* **2012** 981758

[21] Gashti M P, Asselin J, Barbeau J, Boudreau D and Greener J 2016 A microfluidic platform with pH imaging for chemical and hydrodynamic stimulation of intact oral biofilms *Lab. Chip.* **16** 1412–9

[22] Cao X, Zhang S, Chu D, Wu N, Ma H and Liu Y 2017 A design of spectrophotometric microfluidic chip sensor for analyzing silicate in seawater *IOP Conf. Ser.: Earth Environ. Sci.* **82** 012080

[23] Fang T *et al* 2019 Simultaneous underway analysis of nitrate and nitrite in estuarine and coastal waters using an automated integrated syringe-pump-based environmental-water analyzer *Anal. Chim. Acta.* **1076** 100–9

[24] Floquet C F A *et al* 2011 Nanomolar detection with high sensitivity microfluidic absorption cells manufactured in tinted PMMA for chemical analysis *Talanta* **84** 235–9

[25] Grumann M *et al*, 2005 Optical beam guidance in monolithic polymer chips for miniaturized colorimetric assays *18th IEEE Int. Conf. on Micro Electro Mechanical Systems* pp 108–11

[26] Giustarini D, Rossi R, Milzani A and Dalle-Donne I 2008 Nitrite and nitrate measurement by griess reagent in human plasma: evaluation of interferences and standardization *Meth. Enzymol.* **440** 361–80

[27] Shen Y, Zhang Q, Qian X and Yang Y 2015 Practical assay for nitrite and nitrosothiol as an alternative to the griess assay or the 2,3-diaminonaphthalene assay *Anal. Chem.* **87** 1274–80

[28] Motomizu S and Li Z-H 2005 Trace and ultratrace analysis methods for the determination of phosphorus by flow-injection techniques *Talanta* **66** 332–40

[29] Legiret F-E *et al* 2013 A high performance microfluidic analyser for phosphate measurements in marine waters using the vanadomolybdate method *Talanta* **116** 382–7

[30] Costa B *et al* 2017 Application of flow-injection spectrophotometry to pharmaceutical and biomedical analyses *Spectroscopic Analyses—Developments and Applications* (London: IntechOpen) pp 193–212

[31] Skoog D A, West D M, Holler F J and Crouch S R 2014 *Fundamentals of Analytical Chemistry* 9th edn (Belmont, CA: Cengage Learning)

[32] Rushworth C M, Davies J, Cabral J T, Dolan P R, Smith J M and Vallance C 2012 Cavity-enhanced optical methods for online microfluidic analysis *Chem. Phys. Lett.* **554** 1–14 Dec

[33] Ogilvie I R G, Sieben V, Floquet C F A, Zmijan R, Mowlem M and Morgan H 2010 Solvent processing of PMMA and COC chips for bonding devices with optical quality surfaces *14th Int. Conf. on Miniaturized Systems for Chemistry and Life Sciences* vol 2

[34] Liga A, Morton J A S and Kersaudy-Kerhoas M 2016 Safe and cost-effective rapid-prototyping of multilayer PMMA microfluidic devices *Microfluid. Nanofluid.* **20** 164

[35] Bamshad A, Nikfarjam A and Khaleghi H 2016 A new simple and fast thermally-solvent assisted method to bond PMMA–PMMA in micro-fluidics devices *J. Micromech. Microeng.* **26** 065017

[36] Becker H and Gartner C 2000 Polymer microfabrication methods for microfluidic analytical applications *Electrophoresis* **21** 12–26
[37] Hassan S, Nightingale A M and Niu X 2018 Micromachined optical flow cell for sensitive measurement of droplets in tubing *Biomed. Microdevices* **20** 92
[38] Gomes W 1966 Spectrophotometric determination of nitrite and nitrate in doped potassium chloride crystals *Fresenius' Z. Für Anal. Chem.* **216** 387–91
[39] Ridnour L A, Sim J E, Hayward M A, Wink D A, Martin S M, Buettner G R and Spitz D R 2000 A spectrophotometric method for the direct detection and quantitation of nitric oxide, nitrite, and nitrate in cell culture media *Anal. Biochem.* **281** 223–9
[40] Cleary J, Slater C and Diamond D 2007 Field-deployable microfluidic sensor for phosphate in natural waters *Sensors, 2007 IEEE* pp 1001–4
[41] Taylor J R 1982 *An Introduction to Error Analysis: The Study of Uncertainties in Physical Measurements* (Mill Valley, CA: University Science Books)
[42] Shrivastava A 2011 Methods for the determination of limit of detection and limit of quantitation of the analytical methods *Chron. Young Sci.* **2** 21–25